Analysis and control of the vehicle roll dynamics using Sum Of Squares polynomial approach

Imen Iben Ammar, Moustapha Doumiati, Reine Talj, Abbas Chokor, Mohamed Machmoum

Analysis and control of the vehicle roll dynamics using Sum Of Squares polynomial approach

IBEN AMMAR Imen · DOUMIATI Moustapha · TALJ Reine · CHOKOR Abbas · MACHMOUM Mohamed

Abstract The safety of vehicle travel relies on good stability performance, making vehicle motion control a vital technology in vehicles. This paper focuses on investigating the impact of roll control on vehicle performance, particularly in terms of avoiding rollover and ensuring lateral stability. By introducing a feedback roll moment, the roll motion can be effectively controlled. The paper considers two roll reference generators: a static one aimed at zero roll, and a dynamic one based on the vehicle's lateral acceleration. The static roll reference generator enhances stability by employing a fixed reference, particularly beneficial during routine driving conditions. In contrast, the dynamic roll reference generator continually adapts the roll angle reference in response to real-time vehicle dynamics and driving conditions. These proposed reference generators can be paired with varying suspension systems — static reference could be achieved using semi-active suspensions, while the dynamic one is integrated into advanced active suspension systems, offering heightened adaptability and performance. To address the roll control objectives, this paper proposes a novel Sum Of Squares (SOS) integral polynomial tracking control. The proposed controller satisfies control bounds and considers control constraints during the design phase. The effectiveness and robustness of the proposed control scheme are evaluated through numerical simulations using a full vehicle nonlinear model in MATLAB/Simulink. The results of these simulations are compared to super-twisting sliding mode and Lyapunov-based controllers.

Keywords Active suspensions, lateral stability, SOS approach, polynomial control, rollover avoidance.

IBEN AMMAR Imen · DOUMIATI Moustapha (Corresponding author)
ESEO-Tech, 10 Bd Jeanneteau - CS 90717,Angers, 49107, France; Institut de Recherche en Énergie Électrique de Nantes Atlantique, IREENA UR 4642, 37 Boulevard de l'Université - BP406, Saint-Nazaire, F-44602, France.
Email: moustapha.doumiati@eseo.fr
TALJ Reine
Sorbonne universités, Université de Technologie de Compiègne, CNRS, Heudiasyc UMR 7253, CS 60 319, 60 203 Compiègne, France.
CHOKOR Abbas
Continental, 17 Rue Paulin Talabot, 31100 Toulouse.
MACHMOUM Mohamed
Institut de Recherche en Énergie Électrique de Nantes Atlantique, IREENA UR 4642, 37 Boulevard de l'Université - BP406, Saint-Nazaire, F-44602, France.
◇

1 Introduction

The roll motion of the vehicle plays a significant role in various vehicle performances, including ride comfort, road adhesion, lateral stability, and rollover prevention. This importance is particularly emphasized in critical situations where the roll motion control needs to collaborate with other Advanced Driving Assistance Systems ($ADAS$) within an integrated Global Chassis Control (GCC) architecture. Vehicle suspensions are responsible for achieving different performance objectives related to vibratory isolation, road handling, and ride comfort. Depending on the external power input, vehicle suspensions can be categorized into three types: passive, semi-active, and active [1]-[3]. Recent research has shown increased interest in nonlinear control strategies for active suspensions to handle uncertainties and nonlinear dynamics [4, 5]. This paper aims to propose a method for integrating Active Suspensions ($ASus$) with other vehicle stability controllers to enhance rollover avoidance and maintain lateral stability. By coordinating these systems, the vehicle can operate within a larger stable range while engaging the relevant $ADAS$ controller. This approach effectively extends the functionality of $ASus$ and improves overall vehicle safety.

The connection between roll motion control and the occurrence of rollover is evident, as both are influenced by lateral acceleration. Rollover refers to the phenomenon where the vehicle rotates around the virtual axis connecting the wheels on the same side (left or right). $ADAS$ systems have addressed the vehicle rollover problem through braking (differential or normal), steering, or within a GCC architecture [6]. In [8], the authors propose the use of Direct Yaw Controllers (DYC) where the desired yaw rate switches between two expressions. One expression enhances lateral stability, while the other expression avoids rollover. At the low-level control, the desired yaw rate can be achieved through simple braking, but this approach slows down the vehicle. In contrast, [9] demonstrates better performance by using Active Differential Braking (ADB) to achieve the same objective. Other relevant studies, such as [7], suggest controlling the roll motion using steering and/or braking to prevent rollover, regardless of vehicle maneuverability. Authors in [10] investigate the rollover stability of wheel-hub motors and propose an anti-rollover system for wheel-hub electric vehicles. In [11], the authors propose an observer to estimate roll dynamics and a fuzzy logic controller for roll motion control. Enhancing lateral stability relies on the dynamic coupling between vertical and lateral tire forces [12]. Numerous studies have been conducted on $ASus$ and (semi-)$ASus$ to explicitly improve lateral stability [13–17]. The primary objective is to prevent the saturation of tire lateral forces during cornering, which can lead to lateral skidding of the vehicle. This objective is achieved by controlling the vertical tire forces. However, this task can be challenging, especially in the nonlinear saturated region where an inverse tire/road contact model needs to be evaluated. Researchers in [18–20] propose various approaches to address this challenge, such as controlling the vertical load transfer during cornering or minimizing the vertical displacements of the unsprung masses, as these factors significantly influence lateral forces.

In [21], the authors demonstrate in the frequency domain that controlling the roll angle always enhances lateral stability. The paper also presents the time and frequency domain analysis of

the closed-loop system using direct Lyapunov control and Super-Twisting Sliding Mode controller, showing improvements in roll avoidance and lateral stability using active suspensions. However, these controllers have a drawback in their tuning phase, which relies on a heuristic approach and requires a wide range of driving scenarios to ensure optimal performance. Additionally, the Lyapunov model-based approach necessitates a good understanding of vehicle parameters and the measurement of various vehicle dynamics variables, such as tire forces and side-slip angle, which can be a complex task.

Recently, in [24], the authors propose evolutionary algorithms based on model predictive control for vehicle lateral control and roll motion control. Their approach aims to track the lateral positions, sideslip angle, yaw rate, and load transfer ratio. Another method to improve control performance is presented in [25], where the authors achieve zero dynamics through the design of an input-output linearization controller. They further propose cooperative control to enhance the motion stability of vehicles, utilizing a linear combination of the yaw rate and the sideslip angle as the control output. The research paper given in [23] presents the development of an active roll control system for passenger cars using a roll actuator with an electric motor. The authors focus on understanding the roll dynamics of the vehicle and investigating the characteristics of active roll actuators. They propose the use of the reference model method to establish desired roll states, and model predictive control techniques are employed to regulate the rolling motion effectively.

The advancements observed in various GCC approaches have inspired our research to explore a new synergy that combines rollover avoidance and the achievement of lateral stability goals using active suspensions. It is important to note that the main objective of this study is not to introduce a GCC modular system that coordinates different $ADAS$ as discussed in [22], but rather to focus on controlling roll dynamics and understanding its impact on vehicle stability. To achieve this, a novel Sum Of Squares (SOS)-based polynomial roll motion controller is developed in this paper, considering the presence of roll motion perturbations and uncertainties. The robustness and performance of the proposed controller are thoroughly studied and evaluated. The SOS-based control framework proposed in this work introduces significant innovations in two key aspects. First, it enables the computation of nonlinear control gains using the SOS approach. This allows for the design of control strategies that can effectively handle the nonlinearities present in the system. Second, the framework facilitates the design of nonlinear polynomial control with saturation constraints, ensuring that the control inputs remain within desired limits.

Previous attempts at applying the SOS approach to stability analysis of polynomial systems have been presented in Tanaka et al. [26]. The stability conditions in this approach can be formulated in terms of SOS and solved numerically, partially symbolically, using the SOSTools software [27]. The potential of sum of squares programming for controlling nonlinear vehicle systems using polynomial models has also been explored in [28]. Their study focused on solving the lateral stabilization problem for a nonlinear vehicle system while considering input saturation constraints.

In comparison to the existing literature, this research article proposes a novel control scheme

that relies on polynomial functions to track a dynamic roll reference using active suspension actuators. The main contributions of this work are as follows:

1. Detailed analysis of dynamic roll reference generation: The paper provides a comprehensive analysis of the generation of dynamic roll references. It explores various factors that influence the roll motion and proposes a method to determine the desired roll states based on the vehicle dynamics. In contrast to the static roll reference, which enhances stability by adhering to a fixed or predetermined roll angle reference and is thus less adaptable to sudden changes in driving dynamics, the proposed dynamic roll reference generator continually adapts the roll angle reference based on real-time vehicle dynamics and driving conditions. As demonstrated later in this paper, this dynamic approach implies improved stability and superior handling, especially in varied driving conditions.

2. Development of a new robust integral controller: A novel robust integral controller based on a polynomial approach is developed to control the roll motion. This controller takes into account the nonlinearities and uncertainties in the system and provides improved stability and performance.

3. Consideration of actuator dynamics constraints: The controller design phase takes into consideration the constraints imposed by the actuator dynamics. This ensures that the control inputs remain within the physical limitations of the active suspension actuators.

4. Calculation of controller gains using SeDuMi: The controller gains are calculated not only using SOSTools but also with the aid of SeDuMi, which leads to an automatic computation of the gains. This eliminates the need for delicate and heuristic tuning of the nonlinear controllers, as required in existing studies.

The paper is structured as follows: In Section 2, the vehicle dynamics, particularly the extended bicycle model, are briefly summarized. Section 3 discusses the effect of roll control on the problem of rollover. Section 4 presents the global closed-loop architecture and introduces the polynomial controller. In Section 5, the proposed controller is validated through simulations on a full vehicle nonlinear model. The performance of the developed controller is also compared with other controllers based on direct Lyapunov and sliding mode approaches. Finally, Section 6 provides a conclusion that summarizes the key findings and contributions of this research.

2 Vehicle Models

The literature on vehicle modeling is extensive and encompasses models of varying complexity, tailored to specific applications. Researchers focusing on vehicle stability have developed dynamics models in the horizontal plane, including longitudinal and lateral models [29–31]. Others interested in passenger comfort and road handling have developed quarter, semi, and/or full vertical models to describe roll, pitch, and vibrations of the sprung mass [30]. Numerous full vehicle models have been proposed in the literature, taking into account the interactions between

different dynamics. These models offer a comprehensive understanding of vehicle behavior under various driving conditions, incorporating longitudinal, lateral, and vertical dynamics. They are also valuable for simulating and evaluating different control strategies and aiding in the advancement of vehicle technologies.
For instance, authors in [32] and [33] propose a full nonlinear vehicle model validated using the SCANeR Studio vehicle dynamics simulator. The Pacejka tire model is utilized to characterize tire forces. In this paper, to streamline the presentation, the equations of the full vehicle model will not be presented. Instead, the focus will be on the application of the so-called extended bicycle model for control synthesis.

2.1 Extended Bicycle Model

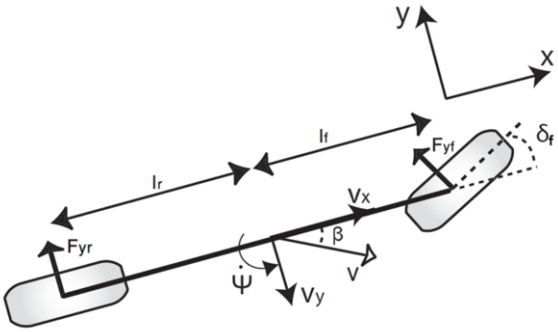

Figure 1: Vehicle bicycle model

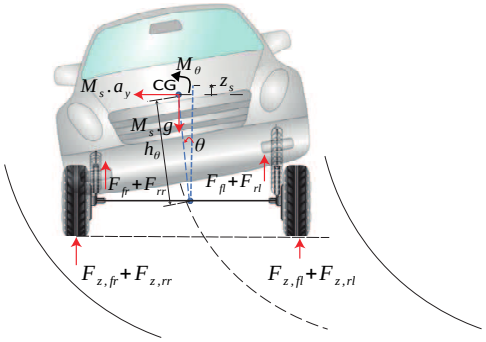

Figure 2: Roll motion (front view)

The extended bicycle model is a vehicle model that integrates the lateral and roll dynamics of the vehicle. It is a simplified linear vehicle model that combines the vehicle's yaw, side-slip, and roll motion dynamics (refer to Figures 1 and 2). The model takes into account the indirect effect of vertical load transfer on tires by incorporating the roll motion in the lateral dynamic equations. Therefore, this coupled lateral-roll vehicle model is valuable for the development of roll angle controllers and for assessing the impact of roll motion control on the vehicle's lateral stability. All the vehicle parameters used in this model are explained in Table 7.2 in

Appendix 7.2. The construction of the extended bicycle model is inspired by the work presented in literature [34] as follows:

$$\begin{aligned} I_z\ddot{\psi} &= F_{yf}l_f + F_{yr}l_r + I_{xz}\ddot{\theta}, \\ MV\left(\dot{\beta}+\dot{\psi}\right) &= F_{yf} + F_{yr} + M_s h_\theta \ddot{\theta}, \\ \left(I_x + M_s h_\theta^2\right)\ddot{\theta} &= M_s h_\theta V\left(\dot{\beta}+\dot{\psi}\right) + (M_s g h_\theta - K_\theta)\theta - C_\theta\dot{\theta} + M_\theta, \end{aligned} \tag{1}$$

where F_{yf} and F_{yr} represent the lateral forces exerted by the tires on the front and rear axles, respectively, and M_θ denotes the active roll moment as a control input. The variables θ, $\dot{\psi}$, V, and β correspond to the vehicle's roll angle, yaw rate, velocity, and sideslip angle, respectively. It is assumed that the lateral forces F_{yf} and F_{yr} have a linear relationship with the side-slip angle of the wheels, yielding:

$$\begin{aligned} F_{yf} &= \mu C_f \alpha_f, \\ F_{yr} &= \mu C_r \alpha_r, \end{aligned} \tag{2}$$

Here, C_f and C_r represent twice the cornering stiffness of the front and rear tires, respectively, and μ denotes the coefficient of road adherence coefficient.
The wheels side-slip angles are determined using the following equations:

$$\begin{aligned} \alpha_f &= -\beta - \tfrac{l_f\dot{\psi}}{V} + \delta_d, \\ \alpha_r &= -\beta + \tfrac{l_r\dot{\psi}}{V}. \end{aligned} \tag{3}$$

where δ_d is the steering angle.

3 Roll motion effect on rollover problem

3.1 Rollover problem description

Vehicle rollover refers to the situation where a vehicle undergoes a rotation of 90 degrees or more around its longitudinal axis, typically initiated by the lifting of two wheels on the same side of the vehicle [35]. The risk of rollover can also be assessed with respect to the axis joining the two remaining wheels in contact with the ground. Although rollover accidents account for a small percentage (3%) of all road accidents, their consequences can be severe, including traumatic brain injuries, broken bones, and fatalities. According to recent statistics from the National Highway Traffic Safety Administration (NHTSA) of the US Department of Transportation [36], approximately 35% of all passenger vehicle crash fatalities are attributed to rollover incidents. The significance of rollover avoidance as a safety concern has been acknowledged by various researchers and automotive organizations [12, 34]. Rollover incidents can occur in two distinct ways: tripped and untripped, as identified by previous studies. Tripped rollover occurs due to external forces acting on the vehicle, while untripped rollover arises from excessive lateral acceleration or roll dynamics in a vehicle equipped with passive suspensions. Untripped rollover can transpire during high-speed cornering or abrupt lane changes and can be predicted by analyzing vehicle dynamics, unlike tripped rollover, which occurs spontaneously.

From the full vehicle model, the roll dynamics is equivalent to:

$$\begin{aligned}\ddot{\theta} =& \frac{1}{I_x + M_s h_\theta^2}[(-F_{fr} + F_{fl})\, t_f + (-F_{rr} + F_{rl})\, t_r + M_s\,(h_\theta\ cos\,(\theta) + z_s)\, a_y \\ &+ M_s\,(h_\theta\ sin\,(\theta) + z_s)\, g + M_\theta],\end{aligned} \tag{4}$$

as shown in Figure 2, where z_s is the sprung mass displacement, a_y is the lateral acceleration, F_{ij} is the passive suspension force on the vehicle corner ij ($i = \{f : front, r : rear\}$ and $j = \{r : right, l : left\}$), and M_θ is the active roll moment to be generated, such as:

$$M_\theta = (-U_{fr} + U_{fl})\, t_f + (-U_{rr} + U_{rl})\, t_r. \tag{5}$$

where U_{ij} represents the suspension actuator active force.

As depicted in Figure 3, the suspension system and tires undergo dynamic motions and vibrations that depend on the deflections of the suspension and tires, as well as the vertical displacements of the sprung and unsprung masses. At each corner ij of the vehicle, the dynamic equations for the suspension and tire system can be expressed as follows:

$$F_{ij} = -K_{s,ij}(z_{s,ij} - z_{us,ij}) - C_{s,ij}(\dot{z}_{s,ij} - \dot{z}_{us,ij}) \tag{6}$$

$$F_{z,ij} = -K_{t,ij}(z_{us,ij} - z_{r,ij}) - C_{t,ij}(\dot{z}_{us,ij} - \dot{z}_{r,ij}), \tag{7}$$

$$F_{s,ij} = F_{ij} + U_{ij}, \tag{8}$$

where $K_{s,ij}$, $C_{s,ij}$, $K_{t,ij}$, and $C_{t,ij}$ are the suspension stiffness, suspension damping, tire stiffness, and tire damping coefficients, respectively. $z_{s,ij}$, $z_{us,ij}$, and $z_{r,ij}$ represent the vertical displacements of the sprung mass, unsprung mass, and the road profile, respectively. $F_{s,ij}$ denotes the total suspension force, which is the sum of passive and active suspension forces.

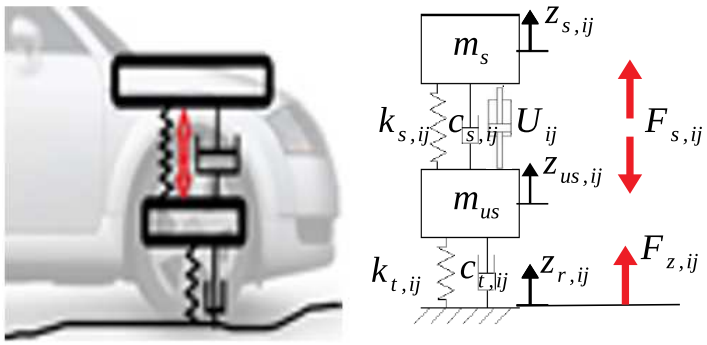

Figure 3: Quarter vehicle vertical model

The roll angle of a vehicle is primarily influenced by the passive suspension forces F_{ij} and the lateral acceleration a_y, as indicated by the roll dynamics equation (4). During high-speed cornering, the lateral acceleration increases, resulting in the induced roll angle shifting towards the outside of the corner. This poses a risk of rollover for the vehicle. To mitigate this risk, an active roll moment M_θ needs to be generated to counteract the roll motion.

3.2 Dynamic Untripped Rollover

The suspension system of a vehicle introduces flexibility, which implies that it cannot be treated as a rigid body. In order to analyze the motion during a rollover event, the vehicle is simplified to have one degree of freedom, represented by the roll angle θ between the suspended and unsuspended masses. This simplified model is depicted in Figure 2. By taking the moments of all forces around the axis that joins the outer wheels (according to Newton's law), the equilibrium is maintained prior to the vehicle initiating a rollover if the following condition is met:

$$M_s a_y h - M_s g(t_f - (h - h_r)sin\theta) + F_{zi} 2t_f = 0. \tag{9}$$

The equation (9) includes the inner vertical force F_{zi}, which represents the sum of the vertical forces exerted by each pair of tires on the same side of the vehicle. As the vehicle speed V increases or the turn radius R decreases, the lateral acceleration a_y also increases. The equilibrium described in (9) is maintained by a natural decrease in F_{zi} while ensuring that a_y remains within certain limits. Eventually, F_{zi} reaches zero, indicating that the inner wheels have lifted off the ground. By assuming small angles, the equation can be simplified to:

$$a_{y,\text{lift-off}} = \frac{t_f - (h - h_r)\theta}{h} g, \tag{10}$$

where $a_{y,\text{lift-off}}$ represents the minimum lateral acceleration that leads to wheels lift-off. This analysis does not account for the transient response of θ, which could lead to a roll overshoot and increase the risk of rollover even at lower lateral accelerations. Additionally, uncertainties such as measurement errors, changes in tires or ground contact surfaces, and vertical shifts in the center of gravity, which could contribute to rollover, are not considered. To ensure safe driving, a safety factor of 0.7 is proposed for the total $a_{y,\text{lift-off}}$ calculated in Equation (10). This introduces a new variable, $a_{y,\text{safe}}$, defined as follows:

$$a_{y,\text{safe}} = 0.7 a_{y,\text{lift-off}} = 0.7 \frac{t_f - (h - h_r)\theta}{h} g. \tag{11}$$

If the lateral acceleration exceeds $a_{y,\text{safe}}$, there is a risk of the inner wheels lifting off during cornering, potentially leading to rollover. Therefore, to prevent rollover, the lateral acceleration a_y must be kept below this threshold [21].

The analysis presented in this context provides an alternative way to quantify the rollover risk, which is equivalent to the Load Transfer Ratio (LTR) defined in [30]. The LTR is a measure that indicates the extent of vertical load transfer from the inside to the outside wheels of a vehicle during a turn or cornering. It is defined as the difference between the vertical forces on the right and left side wheels divided by their sum:

$$LTR = \frac{F_{zr} - F_{zl}}{F_{zr} + F_{zl}}. \tag{12}$$

When the inner wheels lift off the ground, the LTR reaches ± 1, indicating a rollover risk. The LTR varies between -1 and 1, and a rollover risk is detected when its absolute value

exceeds a certain threshold $\overline{LTR}$. Conversely, when the LTR is below a lower threshold $\underline{LTR}$, the vehicle is not at risk of rollover.

3.3 Roll Reference Generation

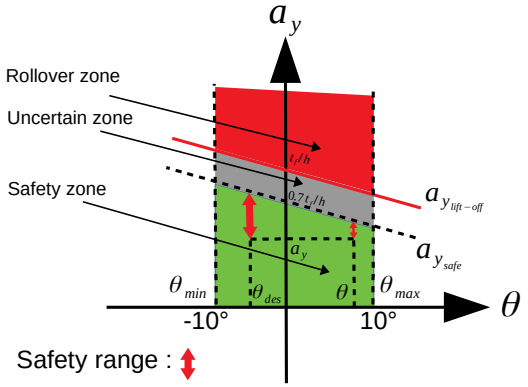

Figure 4: Rollover risk evaluation

In order to prevent rollover situations, the Active Front Steering (AFS) and ADB systems work to reduce the lateral acceleration a_y to keep it below $a_{y_{\text{safe}}}$, while the $ASus$, semi-$ASus$, and Active anti-Roll Bar (ARB) systems aim to increase the maximum safe lateral acceleration $a_{y,\text{safe}}$ by controlling the roll angle [21].

Note that $ASus$s, semi-$ASus$, and ARB are distinct technologies that contribute to managing roll motion in dynamic scenarios [30]. $ASus$ have the capability to apply forces to individual wheels, effectively counteracting the impact of body roll during cornering. Through the independent adjustment of suspension settings for each wheel, active suspensions optimize the vehicle's interaction with the road, minimizing body roll. In comparison, semi-$ASus$ can also adjust damping forces and/or spring rates but are constrained by limitations compared to active suspensions. Their parameter variation is confined within specific limits, and they lack the capacity to actively apply forces to the wheels. ARB function as integral components connecting the left and right wheels of an axle, purposefully designed to resist the vehicle's body roll during cornering. For example, the process of stiffening the semi-$ASus$ or the ARB aims to decrease the vehicle's roll angle towards zero. This procedure establishes ay_{safe}, as evidenced by equation (11), preventing rollover without necessitating a reduction in lateral acceleration. The distinctive contribution of the $ASus$ system lies in its ability to continue turning the roll angle in the negative direction, towards the inner side of the corner. This feature results in a higher shift of ay_{safe}, enhancing safety margins. The desired roll angle, θ_{des}, is thus determined as follows:

- It is set to 0° at zero lateral acceleration (on a straight road).
- It is set to the maximum achievable roll angle 10° (based on vehicle design constraints [37]) at a lateral acceleration equal to the maximum static safe lateral acceleration threshold $0.7\frac{t_f}{h}g$.
- To ensure a smooth transition, a linear mapping between θ_{des} and a_y is desired. Therefore,

the appropriate roll angle θ_{des} is formulated as:

$$\theta_{\text{des}} = -\frac{10\frac{\pi}{180}}{0.7\frac{t_f}{h}g}a_y. \tag{13}$$

Figure 4 illustrates the safety range, which represents the difference between the vehicle's lateral acceleration and the maximum safe lateral acceleration as a function of the vehicle's roll angle. The figure also demonstrates that adjusting the vehicle's roll angle towards θ_{des} as defined in Equation (13) has a more significant effect on increasing the safety range compared to minimizing the roll angle towards zero ($\theta_{\text{des}} = 0$). Based on the analysis given above, the strategic control of roll motion in the opposite direction could play a central role in vehicle dynamics control, offering a multitude of benefits. These include enhanced lateral stability, prevention of rollover incidents, optimized tire contact for improved traction, and adaptive response to diverse driving conditions. Let's resume the key aspects:

- Counteracting forces: by actively controlling roll motion in the opposite direction, the vehicle's suspension system applies forces to counteract lateral forces arising from dynamic maneuvers.This counteraction plays a crucial role in maintaining a more balanced and stable posture for the vehicle.
- Preventing rollover incidents: actively managing roll contributes to maintaining the vehicle's stability, lowering the tendency to tip over, and thereby mitigating the risk of rollover incidents, particularly in scenarios with high lateral forces.
- Optimizing tire contact and traction: control of roll ensures optimal contact between the tires and the road surface during lateral movements.
- Real-time adjustments: the active control of roll allows the vehicle to make real-time adjustments, adapting dynamically to changing driving conditions.

Simulations given in Section 5 illustrate the significance of controlling roll motion in the opposite direction.

4 Closed-Loop Control Architecture

The primary objective of this section is to develop a new robust controller for roll motion control using SOS (Sum of Squares) techniques. The overall closed-loop control scheme is depicted in Figure 5. It consists of the roll reference generator block developed in subsection 3.3 and the roll control block (polynomial controller). The roll angle error and its first derivative serve as inputs to the roll control block, which generates the control signal M_θ. This control signal can be produced by utilizing the four active forces U_{ij} of the active suspension system (ASus). The process of generating this control signal is performed in the control allocation unit and is described by Equation (14):

$$U_{fl} = 0.5\frac{l_r}{l_f + l_r}\frac{M_\theta}{t_f},\ U_{fr} = -0.5\frac{l_r}{l_f + l_r}\frac{M_\theta}{t_f},\ U_{rl} = 0.5\frac{l_f}{l_f + l_r}\frac{M_\theta}{t_r},\ U_{rr} = -0.5\frac{l_f}{l_f + l_r}\frac{M_\theta}{t_r}, \tag{14}$$

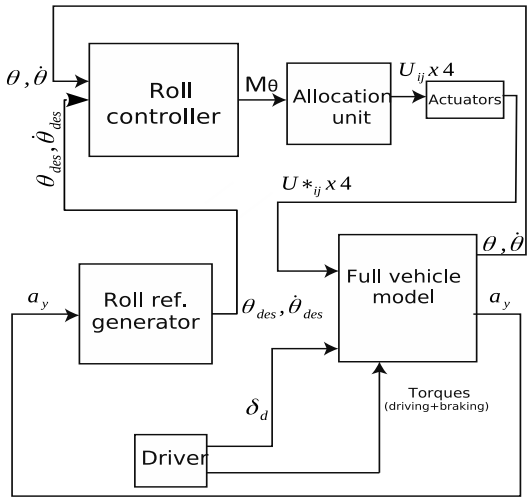

Figure 5: Control scheme

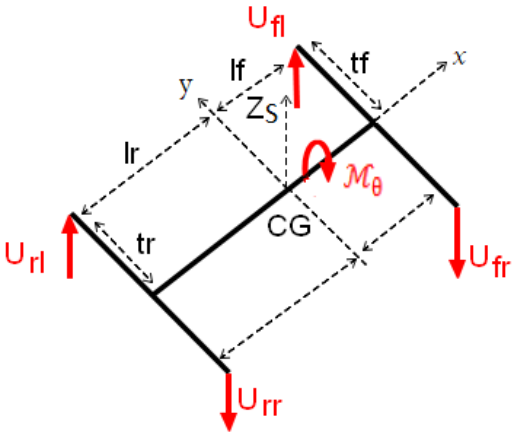

Figure 6: Active forces distribution

This particular distribution of forces is chosen to avoid any influence on the pitch angle and the bounce displacement, as shown in Figure 6. Previous studies in the literature have focused on controlling electro-hydraulic actuators to track a desired force specified by an ASus controller [30]. However, in this paper, we do not delve into the control of the actuator valve. Instead, we employ a simplified actuator model to address the constraints of the actuator, which mainly involve response time (cut-off frequency f) and saturation (maximum achievable force $U_{ij,\max}$). This allows us to obtain a feasible active suspension control input. The actuator model is described by Equation (15):

$$\dot{U}^*_{ij} = 2\pi f * (min(U_{ij}, U_{ij,max}) - U^*_{ij}). \tag{15}$$

One crucial requirement for the actuators is to have a sufficiently high response speed and the ability to generate adequate force to effectively control the vehicle dynamics. The appropriate

selection of actuator characteristics is discussed in [21], where $f = 10$ Hz and $U_{ij,\max} = U_{\max} = 4800$ N. As shown in the subsequent sections, the controller gains will be calculated to respect the constraints of the actuator dynamics.

4.1 SOS Preliminaries

In this subsection, several fundamental definitions and lemmas derived from [38] and [39], are presented. These definitions and lemmas play a crucial role in the subsequent stages of the controller design process.

Definition 4.1 A polynomial $\Psi(x(t))$ is a Sum Of Squares (SOS) if there is a set of polynomials $\psi_i(x(t)), i = 1, ..., s$ such that:

$$\Psi(x(t)) \quad = \quad \sum_{i=1}^{s} \psi_i^2(x(t)), \tag{16}$$

Consequently, if $\Psi(x(t))$ is SOS that means $\Psi(x(t)) \geq 0, \forall x(t)$.

Definition 4.2 Define the following subsets of $\mathbb{R}^n$

$$\gamma(W^{-1}(x(t)), 1) = \{x(t) \in \mathbb{R}^n, x^T(t)W^{-1}(x(t))x(t) \leq 1\} \tag{17}$$

where $W(x(t))$ is a symmetric positive polynomial matrix.

Note that $W(x(t))$ is a matrix that depends on the state $x(t)$. As a result, the domains of attraction for the system may have a broader scope, allowing for the exploitation of the stability region in nonlinear systems.

$$\zeta(Y, \overline{u}) = \{x(t) \in \mathbb{R}^n, |Yx(t)| \leq \overline{u}\} \tag{18}$$

where $\zeta(Y, \overline{u})$ is a polyhedral set.

Lemma 4.3 *[38] Let G, $Y \in \mathbb{R}^{n_u \times n}$ be given matrices, for $x(t) \in \mathbb{R}^n$, if $x(t) \in \zeta(Y, \overline{u})$ then*

$$sat(Gx(t), \overline{u}) = co\{N_l Gx(t) + N_l^- Yx(t), l \in [1, \delta]\}; \delta = 2^{n_u} \tag{19}$$

where n_u is the dimension of the vector u, $sat(.)$ denotes the saturation function and co. denotes the convex hull.
Hence, there were $\overline{h}_1 \geq 0, ..., \overline{h}_\delta \geq 0$ with $\sum_{l=1}^{\delta} \overline{h}_l = 1$ in a manner that

$$sat(Gx(t), \overline{u}) = \sum_{l=1}^{\delta} \overline{h}_l \left[N_l G + N_l^- Y\right] x(t) \tag{20}$$

Here, $N_l \in \mathbb{R}^{n_u \times n_u}$ is a diagonal matrix with elements either 1 or 0 and $N_l^- = I_{n_u} - N_l$. There are 2^{n_u} possible matrices of this type.

4.2 Polynomial Controller

As previously mentioned, the primary objective of the robust controller is to drive the nonlinear roll motion, described by Equation (4), to either zero or a desired value θ_{des} as defined in Equation (13). The controller is designed to operate with any arbitrary reference θ_{des} and will be assessed for both zero and non-zero references.
First, let's define:

$$e_\theta = \theta - \theta_{\text{des}}, \tag{21}$$

where e_θ represents the error between the actual roll angle and the desired roll angle. The objective of the control is to minimize the roll error variable e_θ and bring it to zero. To achieve this, the SOS-based design is employed, which is applicable for controlling nonlinear systems described by polynomial functions. In order to apply this design, the trigonometric functions $\cos(\theta)$ and $\sin(\theta)$ in Equation (4) need to be approximated by the following functions:

$$\begin{aligned} \sin(\theta) &\simeq s_1\theta + s_3\theta^3 \\ cos(\theta) &\simeq 1 - \frac{s_1^2}{2}\theta^2 \end{aligned} \tag{22}$$

where $s_1 = 0.9897$ and $s_3 = -0.1460$.
Then, the roll dynamics will be equivalent to:

$$\begin{aligned} \ddot{\theta} =& \frac{1}{I_x + M_s h_\theta^2}[(-F_{fr} + F_{fl})\, t_f + (-F_{rr} + F_{rl})\, t_r + M_s \left(h_\theta \ \left(1 - \frac{s_1^2}{2}\theta^2\right) + z_s \right) a_y \\ &+ M_s \left(h_\theta \ \left(s_1\theta + s_3\theta^3\right) + z_s \right) g + M_\theta] \end{aligned} \tag{23}$$

To build the suggested polynomial controller, it is important to achieve the polynomial model and control input of the rollover. Lets define $x = \begin{bmatrix} \theta & \dot{\theta} \end{bmatrix}^T$, and so the following mathematical model is considered:

$$\dot{x} = A(\theta)x + BM_\theta + F \tag{24}$$

where, $A(\theta) = \begin{bmatrix} 0 & 1 \\ D_1 M_s g h_\theta \left(s_1 + s_3\theta^2\right) & 0 \end{bmatrix}$, $B = \begin{bmatrix} 0 \\ D_1 \end{bmatrix}$, $D_1 = \frac{1}{I_x + M_s h_\theta^2}$,
$F = G_1 F_{fr} + G_2 F_{fl} + G_3 F_{rr} + G_4 F_{rl} + G_5(\theta, z_s)a_y + G_6 z_s$, $G_1 = \begin{bmatrix} 0 \\ -\mathrm{D_1 t}_f \end{bmatrix}$, $G_2 = -G_1$,
$G_3 = \begin{bmatrix} 0 \\ -\mathrm{D_1 t}_r \end{bmatrix}$, $G_4 = -G_3$, $G_5(\theta, z_s) = \begin{bmatrix} 0 \\ D_1 \left[M_s h_\theta \left(1 - \frac{s_1^2}{2}\theta^2\right) + z_s \right] \end{bmatrix}$, $G_6 = \begin{bmatrix} 0 \\ \mathrm{D_1 M}_s \mathrm{g} \end{bmatrix}$.
As mentioned before, the controller gains are chosen to respect the actuator dynamics constraints $-U_{max} \leq U_{ij} \leq U_{max}$. Then,

$$-M_{\theta,\max} \leq M_\theta \leq M_{\theta,\max} \tag{25}$$

where $M_{\theta,\max} = \min(t_f, t_r)(l_f + l_r)U_{max}/0.5\max(l_f, l_r)$.
To ensure that the active roll moment M_θ is between $-M_{\theta,\max}$ and $M_{\theta,\max}$, we will use the following polynomial system with saturation constraint:

$$\dot{x} = A(\theta)x + Bsat(M_\theta, M_{\theta,\max}) + F \tag{26}$$

where

$$sat(M_\theta,M_{\theta,\max}) = \begin{cases} M_{\theta,\max} & if\ M_\theta > M_{\theta,\max} \\ M_\theta \quad if\ -M_{\theta,\max} \le M_\theta \le M_{\theta,\max} \\ -M_{\theta,\max} & if\ M_\theta < -M_{\theta,\max} \end{cases} \tag{27}$$

We aim to design a polynomial controller that achieves the objective of $\theta \to \theta_{\text{des}}$ as $t \to \infty$. To accomplish this, we consider an augmented polynomial system that includes an output integral error term, which is defined as follows:

$$e_1 = \int (\theta - \theta_{des})\, dt \tag{28}$$

Combining (26) with (28), we obtain the following augmented dynamics system:

$$\begin{cases} \dot{x} = A(\theta)x + Bsat(M_\theta, M_{\theta,\max}) + F \\ \dot{e}_1 = \theta - \theta_{des} \end{cases} \tag{29}$$

The objective of output regulation under saturation constraints, is achieved by stabilizing the system at an equilibrium state that yields $\theta = \theta_{\text{des}}$.
The control law is defined as follows:

$$M_\theta(\theta) = K_1(\theta)x + K_2(\theta)e_1 \tag{30}$$

$K_i(\theta)$, $i = 1, 2$, represent the gains of the controller. θ, $\dot{\theta}$ could be measured by the Inertial Measurement Unit (IMU).
Let $Y(\theta)$ be given as polynomial matrix, we got:

$$x \in \zeta(Y(\theta), M_{\theta,\max}) \tag{31}$$

By applying Lemma 4.3, control law (30) considering actuators saturation constraints can thus be written as:

$$sat(K_1(\theta)x + K_2(\theta)e_1, M_{\theta,\max}) = \sum_{l=1}^{\delta} \overline{h}_l\{(N_l K_1(\theta) + N_l^- Y(\theta))x + (N_l K_2(\theta) + N_l^- Y(\theta))e_1\} \tag{32}$$

with $l \in [1, \delta]$; $\delta = 2^{n_{M_\theta}}$ and n_{M_θ} is the dimension of the control input vector M_θ. Note that in this case study, $n_{M_\theta} = 1$ and we have chosen $N_l = 1$, and so $N_l^- = 0$.
The following augmented dynamics system is considered:

$$\begin{cases} \dot{x} = (A(\theta) + BK_1(\theta))x + BK_2(\theta)e_1 + F \\ \dot{e}_1 = \theta - \theta_{des} \end{cases} \tag{33}$$

Let $\widetilde{x} = \left[x^T,\, e_1\right]^T = \left[\theta,\, \dot{\theta},\, e_1\right]^T$, the polynomial model $\widetilde{x}$ is described as follows:

$$\begin{aligned}\dot{\widetilde{x}} =&\mathbb{A}(\theta)\widetilde{x} + \mathbb{B}sat(M_\theta, M_{\theta,\max}) + \mathbb{G}_1F_{fr} + \mathbb{G}_2F_{fl} + \mathbb{G}_3F_{rr} + \mathbb{G}_4F_{rl} + \mathbb{G}_5(\theta, z_s)a_y + \mathbb{G}_6z_s \\ &+ \mathbb{G}_7\theta_{des}\end{aligned} \tag{34}$$

where $\mathbb{A}(\theta) = \begin{bmatrix} 0 & 1 & 0 \\ D_1M_sgh_\theta\left(s_1 + s_3\theta^2\right) & 0 & 0 \\ 1 & 0 & 0 \end{bmatrix}$, $\mathbb{B} = \begin{bmatrix} 0 \\ D_1 \\ 0 \end{bmatrix}$, $\mathbb{G}_1 = \begin{bmatrix} 0 \\ -D_1t_f \\ 0 \end{bmatrix}$,

$\mathbb{G}_2 = \begin{bmatrix} 0 \\ D_1t_f \\ 0 \end{bmatrix}$, $\mathbb{G}_3 = \begin{bmatrix} 0 \\ -D_1t_r \\ 0 \end{bmatrix}$, $\mathbb{G}_4 = \begin{bmatrix} 0 \\ D_1t_r \\ 0 \end{bmatrix}$,

$\mathbb{G}_5(\theta, z_s) = \begin{bmatrix} 0 \\ D_1\left[M_sh_\theta\left(1 - \frac{s_1^2}{2}\theta^2\right) + z_s\right] \\ 0 \end{bmatrix}$, $\mathbb{G}_6 = \begin{bmatrix} 0 \\ \mathrm{D_1M_sg} \\ 0 \end{bmatrix}$, $\mathbb{G}_7 = \begin{bmatrix} 0 \\ 0 \\ -1 \end{bmatrix}$.

The polynomial controller is derived in the following manner:

$$\begin{aligned}M_\theta(\theta) =&\mathbb{K}(\theta)\widetilde{x} \\ =&K_1(\theta)x + K_2(\theta)e_1 \\ =&K_{11}(\theta)\theta + K_{12}(\theta)\dot{\theta} + K_2(\theta)e_1\end{aligned} \tag{35}$$

where $\mathbb{K}(\theta) = \begin{bmatrix} K_{11}(\theta) & K_{12}(\theta) & K_2(\theta) \end{bmatrix}$.

Substituting (35) into (34), the closed-loop system is represented as follows:

$$\begin{aligned}\dot{\widetilde{x}} =&\left\{\mathbb{A}(\theta) + \mathbb{B}\mathbb{K}(\theta)\right\}\widetilde{x} + \mathbb{G}_1F_{fr} + \mathbb{G}_2F_{fl} + \mathbb{G}_3F_{rr} + \mathbb{G}_4F_{rl} + \mathbb{G}_5(\theta, z_s)a_y + \mathbb{G}_6z_s + \mathbb{G}_7\theta_{des} \\ =&\mathbb{H}(\theta)\widetilde{x} + \mathbb{G}_1F_{fr} + \mathbb{G}_2F_{fl} + \mathbb{G}_3F_{rr} + \mathbb{G}_4F_{rl} + \mathbb{G}_5(\theta, z_s)a_y + \mathbb{G}_6z_s + \mathbb{G}_7\theta_{des}\end{aligned} \tag{36}$$

where $\mathbb{H}(\theta) = \mathbb{A}_1(\theta) + \mathbb{B}_1\mathbb{K}(\theta)$. The regulator design aims to determine the polynomial gains $\mathbb{K}(\theta)$ such that the closed-loop system is stable, and the output θ asymptotically converges to θ_{des}. The stability analysis result is summarized in the following theorem.

Theorem 4.4 *Let $S > 0$ be a diagonal matrix. The polynomial system described by Equation (34) can be stabilized using a polynomial controller that adheres to the constraint (27), provided that there exists a polynomial positive symmetric matrix $P(\overline{\widetilde{x}})$ (where $\overline{\widetilde{x}} = [\theta, e_1]$), polynomial matrices $Z(\theta)$ and $T(\theta)$, and positive scalars $\varepsilon_i(\widetilde{x}) > 0$ for $i = 1, 2, 3$. These conditions must satisfy the following SOS-based conditions:*

$$v_1^T(P(\overline{\widetilde{x}}) - \varepsilon_1(\overline{\widetilde{x}})I)v_1, \quad is \quad SOS \tag{37}$$

$$v_2^T\left(\begin{bmatrix} M_{\theta,\max_r}^2 & T_r(\theta) \\ * & P(\overline{\widetilde{x}}) \end{bmatrix} - \varepsilon_2(\overline{\widetilde{x}})I\right)v_2 \quad is \quad SOS \tag{38}$$

$$-v_3^T(\Omega(\widetilde{x}) + \varepsilon_3(\widetilde{x})I)v_3 \quad is \quad SOS \tag{39}$$

where v_i, (i=1,2,3), denote symbolic decision vectors that are independent of $\widetilde{x}$ and to be declare using Symbolic Math Toolbox (The decision vectors are meant to be unknown vectors), $T_r(\theta)$ denotes the rth row of $T(\theta)$ and $M_{\theta,\max_r}$ is the rth row of $M_{\theta,\max}$, $r = 1, ..., n_{M_\theta}$,

$$\Omega(\widetilde{x}) = \begin{bmatrix} \Omega^1(\widetilde{x}) & P(\overline{\widetilde{x}})S \\ SP(\overline{\widetilde{x}}) & -P(\overline{\widetilde{x}}) \end{bmatrix} \tag{40}$$

$$\begin{aligned} \Omega^1(\widetilde{x}) &= \mathbb{A}(\theta)P(\overline{\widetilde{x}}) + \mathbb{B}Z(\theta) + Z^T(\theta)\mathbb{B}^T + P(\overline{\widetilde{x}})\mathbb{A}^T(\theta) - \sum_{q\in Q} \frac{\partial P(\overline{\widetilde{x}})}{\partial \widetilde{x}_{1_q}} \mathbb{A}^q(\theta)\widetilde{x} \\ &\quad + \mathbb{G}_1\mathbb{G}_1^T + \mathbb{G}_2\mathbb{G}_2^T + \mathbb{G}_3\mathbb{G}_3^T + \mathbb{G}_4\mathbb{G}_4^T + \mathbb{G}_5(\theta, z_s)\mathbb{G}_5^T(\theta, z_s) + \mathbb{G}_6\mathbb{G}_6^T + \mathbb{G}_7\mathbb{G}_7^T \end{aligned}$$

A stabilizing feedback gain $\mathbb{K}(\theta)$ can be obtained from $P(\overline{\widetilde{x}})$ and $Z(\theta)$ as $\mathbb{K}(\theta) = Z(\theta)P^{-1}(\overline{\widetilde{x}})$.

Remark 4.5 In SOS condition (39), by introducing a diagonal matrix S, we can obtain polynomial gains $\mathbb{K}(\theta)$ that result in improved performance. By appropriately choosing the diagonal elements of S, we can achieve a faster decay rate for the regulation error.

To analyze the convergence of the system (36), we consider a polynomial Lyapunov function given by:

$$V(\widetilde{x}) = \widetilde{x}^T P^{-1}(\overline{\widetilde{x}})\widetilde{x} \tag{41}$$

Here, as per Theorem 4.4, $P^{-1}(\overline{\widetilde{x}})$ is a positive definite symmetric polynomial matrix in $\overline{\widetilde{x}}$, where $\overline{\widetilde{x}} = [\theta, e_1]$. In order to avoid introducing non-convex conditions, we assume that $P^{-1}(\overline{\widetilde{x}})$ only depends on states $\overline{\widetilde{x}}$ that are not directly affected by the control input. In other words, it only depends on states whose corresponding rows in $\mathbb{B}$ are zero.
Taking the time derivative of $V(\widetilde{x})$ along the control dynamics (36) results in

$$\dot{V}(\widetilde{x}) = \dot{\widetilde{x}}^T P^{-1}(\overline{\widetilde{x}})\widetilde{x} + \widetilde{x}^T P^{-1}(\overline{\widetilde{x}})\dot{\widetilde{x}} + \widetilde{x}^T \dot{P}^{-1}(\overline{\widetilde{x}})\widetilde{x} \tag{42}$$

Therefore to calculate the gains $K_i(\theta)$, the following condition must be respected :

$$\dot{V}(\widetilde{x}) \leq -\widetilde{x}\overline{S}\widetilde{x} + F_{fr}^T F_{fr} + F_{fl}^T F_{fl} + F_{rr}^T F_{rr} + F_{rl}^T F_{rl} + a_y^T a_y + z_s^T z_s + \theta_{des}^T \theta_{des} \tag{43}$$

This implies that $\dot{V}(\widetilde{x}) \leq 0$ for $\lambda_{\min}(\overline{S})\|\widetilde{x}\|^2 \geq \|F_{fr}\|^2 + \|F_{fl}\|^2 + \|F_{rr}\|^2 + \|F_{rl}\|^2 + \|a_y\|^2 + \|z_s\|^2 + \|\theta_{des}\|^2$ (where $\lambda_{\min}(.)$ represents the minimum eigenvalue operator).
The system's Lyapunov stability condition $V(\widetilde{x}) > 0$ and $\dot{V}(\widetilde{x}) \leq 0$ guarantees the boundedness of $\widetilde{x}$, where $\widetilde{x} = \left[\theta, \dot{\theta}, e_1\right]^T$. Consequently, the boundedness of the states θ, $\dot{\theta}$ and e_1, is ensured. Furthermore, the boundedness of both $\dot{\theta}$ and $\dot{\theta}_{\text{des}}$ dictate the boundedness of the second derivative of e_1, $\ddot{e}_1 = \dot{\theta} - \dot{\theta}_{\text{des}}$. Indeed, $\dot{\theta}_{\text{des}}$ could be either 0 - if θ_{des} is 0 - or function of the jerk according to equation (13) and thus it is constrained for comfort and safety considerations based on the vehicle dynamics properties [42].
In light of the aforementioned analysis, one can conclude the following:

- $\ddot{e}_1$ is bounded, then $\dot{e}_1$ is uniformly continuous;

- $\dot{e}_1$ is uniformly continuous and e_1 has finite limit as t approaches infinity, then, Barbalat's Lemma [43] ensures the convergence of $\dot{e}_1$ to zero as t tends to infinity, signifying that θ tracks its desired value:

$$\lim_{t\to+\infty} \dot{e}_1 = \lim_{t\to+\infty} (\theta - \theta_{des}) = 0. \tag{44}$$

For more detailed analysis of the system stability, reader could refer to Appendix 7.1, and [38, 41].

5 Controllers Validation and Performance Comparison

In the forthcoming section, the proposed controller's effectiveness will be assessed utilizing the detailed vehicle model presented by the authors in previous references [22], [32], and [33]. This model has undergone thorough validation across a range of driving scenarios through the use of the SCANeR Studio vehicle dynamics professional simulator [44]. The comprehensive model encompasses longitudinal, lateral, and vertical vehicle dynamics, incorporating the complete Pacejka tire model. As a result, it stands as a highly reliable model that takes into consideration various facets of vehicle dynamics, ensuring a precise evaluation of the control approach's performance. To validate the proposed controller's ability to mitigate both lateral instability and rollover risk, the fishhook maneuver will be employed. This maneuver involves a rapid steering motion in one direction, followed by an equally rapid steering motion in the opposite direction, as illustrated in Figure 7. By subjecting the vehicle to this challenging maneuver, the control approach can be thoroughly tested under demanding conditions. Furthermore, sinusoidal disturbances with a frequency of 8 rad/s and an amplitude of 4 mm will be introduced to simulate small irregularities in the road profile. These disturbances help assess the controller's ability to handle external perturbations and maintain stability in real-world driving scenarios.

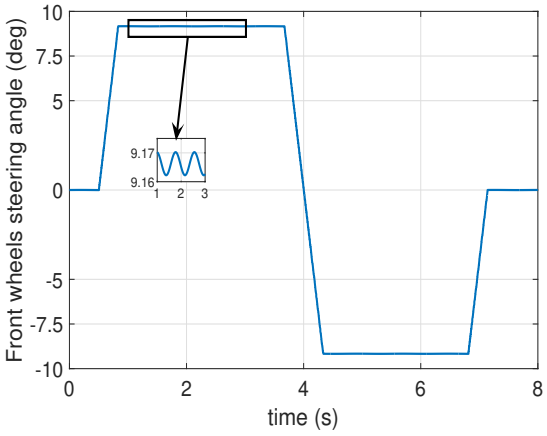

Figure 7: Fishhook steering

The vehicle initial speed is $V = 120\ km/h$, while the throttle and the braking pedals are dropped. In the next, the performances of the proposed polynomial controller (PC) will be evaluated and compared to Lyapunov and sliding mode controllers. For this purpose, the next subsection briefly presents the corresponding control laws given in [21].

5.1 Lyapunov and Super-Twisting Sliding Mode controllers

In [21], a controller based on Lyapunov function has been proposed. The design process of the controller ensures intrinsic stability, which is demonstrated throughout the paper.
The control input M_θ using Lyapunov approach gives:

$$\begin{aligned} M_\theta = \quad & (I_x + M_s h_\theta^2)[-M_{\theta_{eq}} + \ddot{\theta}_{des} - (\alpha_\theta + k_{1\theta})(\dot{\theta} - \dot{\theta}_{des}) - (\alpha_\theta k_{1\theta} + k_{2\theta})(\theta - \theta_{des}) \\ & -\alpha_\theta k_{2\theta} \textstyle\int_0^t (\theta - \theta_{des}) d\tau], \end{aligned} \tag{45}$$

where

$$M_{\theta_{eq}} = \frac{1}{I_x + M_s h_\theta^2}[(-F_{fr} + F_{fl})t_f + (-F_{rr} + F_{rl})t_r + M_s(h_\theta cos(\theta) + z_s)a_y + M_s(h_\theta sin(\theta) + z_s)g] \tag{46}$$

Implementing this control input requires the measurement or estimation of various vehicle parameters and variables, which can present challenges for real-time implementation of the controller. The feed-forward command, consisting of $-M_{\theta eq}$ and $(I_x + M_s h\theta^2)$, compensates for all the dynamics of the roll angle expressed in equation (4), in addition to the robust feedback terms on e_θ, its time derivative, and the integral of equation (45). The Inertial Measurement Unit (IMU) measures θ, $\dot{\theta}$, and a_y, while the suspension forces F_{ij} can be estimated from the deflections of the suspensions. Obtaining z_s requires appropriately tuned filters or observers.
Another controller based on the Super-Twisting Sliding Mode ($STSM$) technique has been developed [21]. $STSM$ is a second-order sliding mode control method that handles a relative degree equal to one. It aims to drive the system states to reach a sliding surface within a finite time and stay on this surface to ensure good tracking even in the presence of disturbances. However, one drawback of $STSM$ is the potential occurrence of chattering once the equilibrium is reached, which can have a negative impact on the health of the actuators. The sliding mode based control law, based on the Super-Twisting algorithm, is presented in [21] and can be described as follows:

$$M_\theta = -\alpha_\theta |s_\theta|^{0.5} \frac{s_\theta}{|s_\theta| + \varepsilon} - \beta_\theta \int_0^t \frac{s_\theta}{|s_\theta| + \varepsilon} d\tau \tag{47}$$

where s_θ is the sliding surface, α_θ and β_θ are positive gains carefully chosen to ensure finite-time convergence. To reduce the chattering effect, an approximation function $\frac{s_\theta}{|s_\theta|+\varepsilon}$ is applied, where ε is a small positive value. It is worth noting that unlike the Lyapunov-based controller mentioned earlier, the developed $STSM$ controller formulated here can be considered as a model-free controller as it neglects the control equivalent term of the control input.
For both the Lyapunov-based and $STSM$ controllers, the selection of the controller gains has been performed through multiple simulation tests under different scenarios. It should be acknowledged that finding the appropriate gains for these two approaches is not a straightforward

task. In the context of PC design using the SOS approach, the controller gains are automatically calculated, as discussed in the next subsection. This feature not only saves time but also contributes to more reliable and robust outcomes. For the simulation phase, we will use the same values of the controller gains as those found in [21] for the Lyapunov-based and $STSM$ controllers.

5.2 Simulation results in nominal conditions

5.2.1 Polynomial controller gains

For the simulations, the vehicle parameter values given in Table 7.2 are considered (see Appendix 7.2). The tuning matrix S (see Theorem 1) is chosen equal to $diag\{0.02, 0.0085, 4.02\}$. The determination of the controller gains involves the essential contribution of two MATLAB toolboxes, SOSTools and SeDuMi. SOSTools to resolve Sum of Squares (SOS) optimization problems, whereas SeDuMi is specifically designed to handle linear matrix inequalities (LMIs) [45, 46]. When dealing with Sum Of Squares Programs (SOSPs), a strategic transformation into SemiDefinite Programs (SDPs) is a key step. SOSTools seamlessly executes this conversion process. In the realm of LMIs, SeDuMi assumes a crucial role by automatically computing gains as an integral part of the solution. This feature of SeDuMi significantly offers benefits such as efficiency, numerical stability, and versatility. Using Theorem 4.4, to articulate and address the Sum Of Squares Program (SOSP) using SOSTOOLS, the process involves the following steps: 1) Initialization of the SOSP, 2) Declaration of the SOSP variables, 3) Definition of the SOSP constraints, 4) Utilization of the "*sossolve*" command to invoke the solver (e.g., SeDuMi), which transforms the SOSP into an equivalent SemiDefinite Program (SDP). The solver then processes this SDP and reverts the obtained result back into solutions for the original SOSP. 5) Retrieval of the feasible solutions. As results:

$$P(\theta) = \begin{bmatrix} P_{11}(\theta) & P_{12}(\theta) & P_{13}(\theta) \\ * & P_{22}(\theta) & P_{23}(\theta) \\ * & * & P_{33}(\theta) \end{bmatrix} \tag{48}$$

$$\begin{aligned} P_{11}(\theta) &= 5769\theta^2 + 1.791 \times 10^5 \\ P_{12}(\theta) &= 20220\theta^2 - 8.067 \times 10^5 \\ P_{13}(\theta) &= -835.6\theta^2 - 11240 \\ P_{22}(\theta) &= 1.303 \times 10^7\theta^2 + 2.003 \times 10^7 \\ P_{23}(\theta) &= -19390\theta^2 - 6758 \\ P_{33}(\theta) &= 1258\theta^2 + 1396 \end{aligned}$$

The obtained polynomial control gain is given as follows

$$\mathbb{K}(\theta) = Z(\theta)P^{-1}(\theta) \tag{49}$$

with

$$Z(\theta) = \begin{bmatrix} Z_1(\theta) & Z_2(\theta) & Z_3(\theta) \end{bmatrix} \tag{50}$$

$$
\begin{aligned}
Z_1(\theta) &= -9.287 \times 10^9 \theta^2 - 1.593 \times 10^{10} \\
Z_2(\theta) &= -9.6 \times 10^9 \theta^2 - 8.52 \times 10^9 \\
Z_3(\theta) &= 2.518 \times 10^7 \theta^2 + 7.149 \times 10^8
\end{aligned}
$$

5.2.2 Controllers validation: static θ_{des}

This section compares the performance of three controllers, namely $STSM$, Lyapunov-based (developed in [21]), and polynomial controllers, with the objective of minimizing the roll angle to $\theta_{des} = 0$.

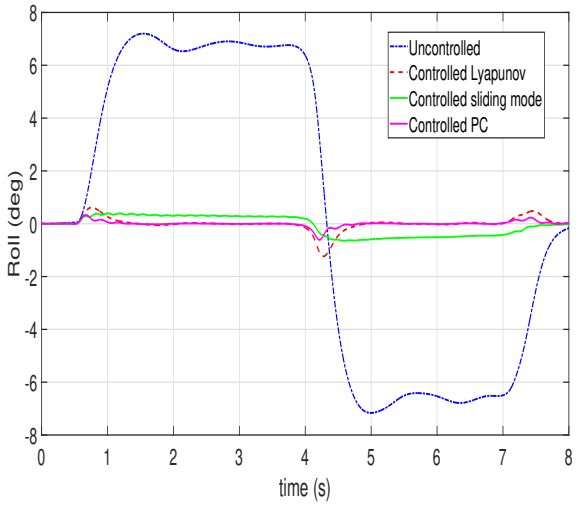

Figure 8: Roll comparison; $\theta_{des} = 0$

The roll angle comparison is depicted in Figure 8. The plot shows the roll angle of a vehicle equipped with passive suspensions (uncontrolled roll), which reaches up to 7° in both directions. All three controllers exhibit efficient performance in reducing the roll angle towards zero. In contrast, the Lyapunov-based controller, in addition to its robust feedback control law (45), compensates for all the dynamics of the roll angle to achieve this level of performance [21]. This implies that a comprehensive understanding of the components of $M_{\theta_{eq}}$ is necessary in real-world applications, including parameters identification, estimation, ideal modeling, and measurement. On the other hand, the polynomial controller (PC) effectively controls the roll angle by generating feedback from the roll angle itself (35), without requiring compensation for roll dynamics. This characteristic is a result of the robustness of the polynomial control law. Consequently, the polynomial controller holds an advantage over the Lyapunov-based controller, particularly in real-time applications where estimations and measurements may be imprecise, and the vehicle system may be subject to disturbances. The $STSM$ controller also exhibits satisfactory performance in controlling the roll angle towards zero. This is observed in the results. Additionally, Figure 9 illustrates the lateral acceleration of the vehicle without any

control. It can be noted that the lateral acceleration remains approximately the same for all the roll controllers. The main objective of the controllers is to increase the maximum safe lateral acceleration, as indicated in (11), which depends on the roll angle. Hence, minimizing the roll angle towards zero effectively enhances the maximum safe lateral acceleration, as demonstrated in the same figure. However, it becomes evident that roll control alone is insufficient at higher lateral accelerations, which may occur due to higher speeds or sharper road curvatures. In such cases, additional control strategies are necessary to ensure the vehicle's stability and safety.

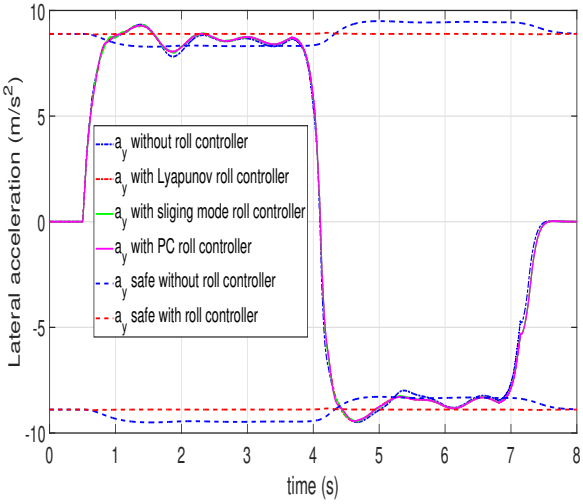

Figure 9: ay comparison; $\theta_{des} = 0$

Figure 10 presents the lateral stability of the vehicle represented by its "Stability Index" (SI), which is determined based on the side-slip angle and its rate of change. The expression for SI is provided in Equation (51), where the values of q_1 and q_2 depend on the specific vehicle parameters and road conditions:

$$SI = |q_1\beta + q_2\dot{\beta}|. \tag{51}$$

The SI value is normalized and ranges from 0 to 1. A threshold $\underline{SI}$ indicates stable driving conditions, while a threshold $\overline{SI}$ signifies critical lateral stability. When the SI value exceeds $\overline{SI}$, the vehicle enters an unstable region. Estimating the side-slip angle β and its velocity $\dot{\beta}$ is necessary for the utilization of the SI criterion in monitoring. Figure 10 demonstrates that the uncontrolled roll vehicle exhibits a lateral SI exceeding 0.7. However, the introduction of the proposed controllers significantly improves lateral stability. Although the improvement is not sufficient to bring the SI below 0.7, minimizing the roll angle to zero can complement the other controllers, such as AFS and the DYC, in a coordinated strategy known as the GCC. This approach helps to prevent lateral skidding and enhance overall vehicle stability.

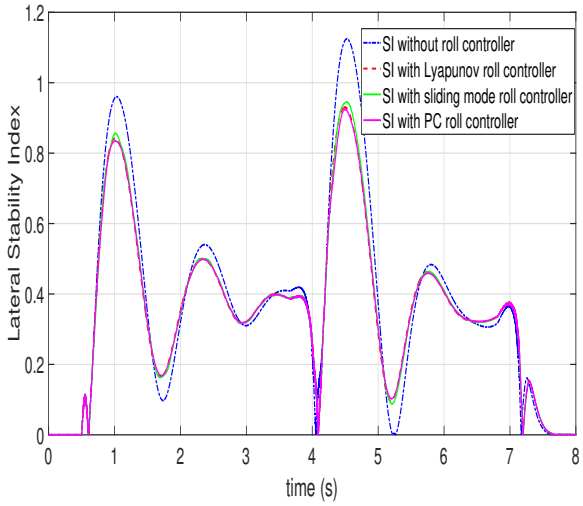

Figure 10: SI comparison; $\theta_{des} = 0$

5.2.3 Controllers validation: dynamic θ_{des}

In this section, the controllers' performance will be evaluated while controlling the roll angle θ towards the desired angle θ_{des} in the opposite direction, as indicated by Equation (13). Similar to Figure 8, Figure 11 illustrates the roll angle for the uncontrolled case, the desired trajectory, and the roll angle under the influence of the controllers. The Lyapunov-based, PC, and $STSM$ controllers effectively track the desired roll trajectory. However, the $STSM$ controller exhibits some error due to its lack of knowledge about the roll dynamics. This transient behavior can be improved by considering the equivalent control input. Taking into account the equivalent control input can enhance the $STSM$ controller's performance and reduce the tracking error in the roll angle.

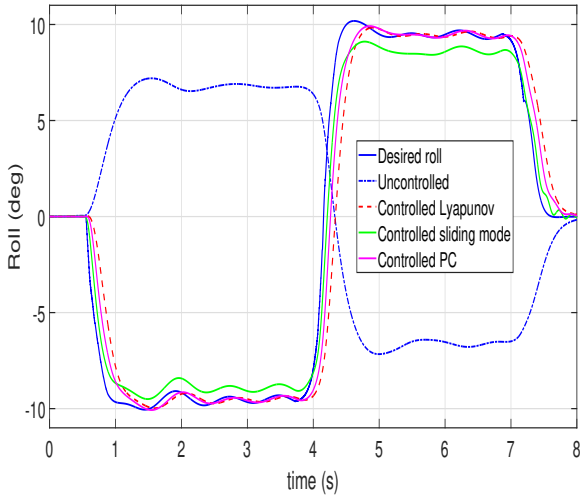

Figure 11: Roll comparison; θ_{des} opposite direction

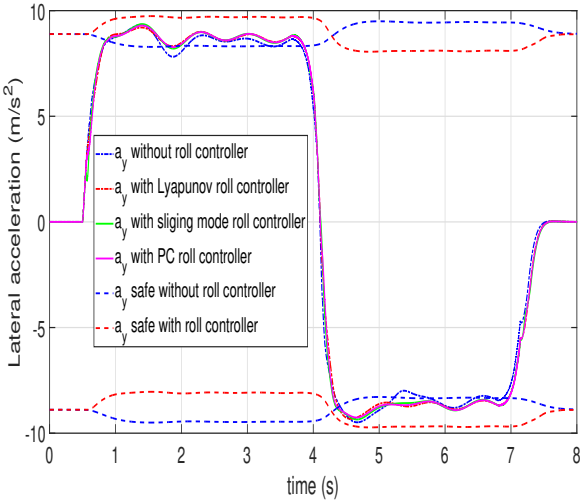

Figure 12: ay comparison; θ_{des} opposite direction

Figure 12 presents the lateral accelerations of both the uncontrolled roll vehicle and the controlled vehicles. It is evident that the maximum safe lateral acceleration is increased compared to the case where the roll angle is minimized to zero. This improvement eliminates the risk of rollover within this range of lateral acceleration. Furthermore, Figure 13 illustrates the LTR for the uncontrolled roll vehicle, which reaches a value of 1 (or -1), indicating a significant risk of rollover. However, for the roll-controlled vehicles (Lyapunov-based, polynomial, and sliding mode), the LTR is improved and reduced to 0.85 (or -0.85). The reduction in LTR signifies enhanced stability and a decreased likelihood of rollover for the controlled vehicles compared to

the uncontrolled vehicle. The controllers effectively mitigate the risk of rollover by regulating the roll angle and its dynamics.

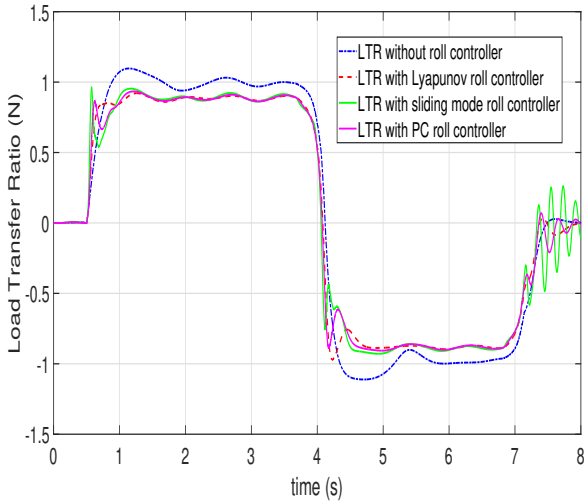

Figure 13: LTR comparison; θ_{des} opposite direction

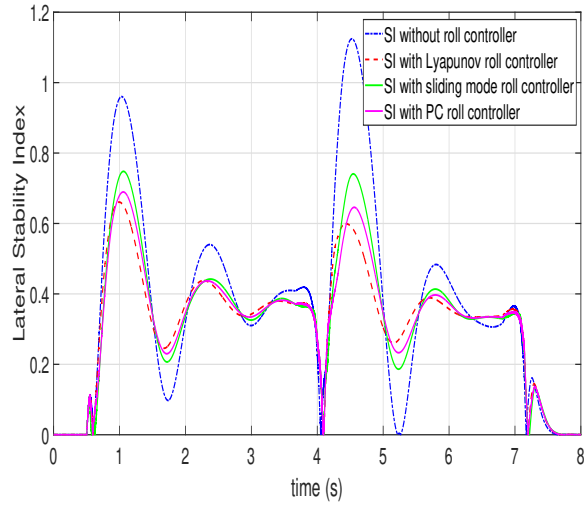

Figure 14: SI comparison; θ_{des} opposite direction

In Figure 14, the lateral stability of the uncontrolled roll vehicle is shown to exceed the threshold value of 0.7 and reach as high as 1.14, indicating a loss of lateral stability. This situation arises due to the vehicle experiencing high lateral acceleration that surpasses the limit of lateral acceleration handling ($\mu.g$) [30]. Additionally, the insufficient lateral forces on the inner tires, caused by low vertical loads, exacerbate this condition. However, when the roll angle is controlled towards the inside wheels, the vertical forces on these tires increase, resulting in higher

lateral forces and improved lateral stability, as depicted in the same figure. Therefore, the $ASus$ system plays a crucial role in maintaining the vehicle's lateral stability, particularly after sharp steering maneuvers, as the different roll controllers reduce SI to 0.7 or below. Figure 15 shows that the longitudinal speed of the vehicle consistently decreases during all the tests at a constant rate. This decrease in speed is attributed to frictional losses and the aggressive steering maneuvers. It is important to note that the roll control implemented in this study aims to prevent rollover and lateral skidding, and it does not directly affect the vehicle's speed. Other stabilization controllers, such as Active Differential Braking (ADB), can have an impact on the vehicle's speed [30].

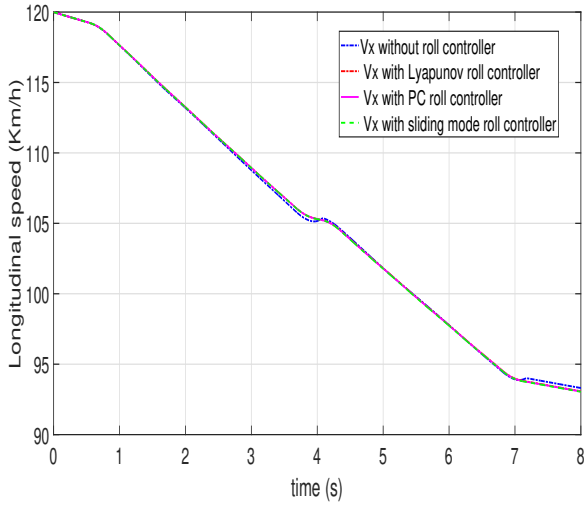

Figure 15: Vx comparison; θ_{des} opposite direction

Figure 16 demonstrates the benefits of roll control in improving lateral stability and preventing rollover, as evident from the generated trajectories. The trajectories produced by the roll control approach closely align with each other, indicating its superiority over other controllers such as AFS and ADB that are designed to achieve similar objectives, as explained in [30]. In Figure 17, the control inputs for the Lyapunov-based, polynomial, and sliding mode controllers are depicted, which correspond to the forces provided by the $ASus$ actuators. It can be observed that their maximum value is approximately $4000N$, and this value can be achieved without saturation of the $ASus$ actuators. However, it is important to note that the $STSM$ controller exhibits significant chattering between $7s$ and $8s$, resulting in high energy consumption and a lack of driving comfort, as observed from the same figure.

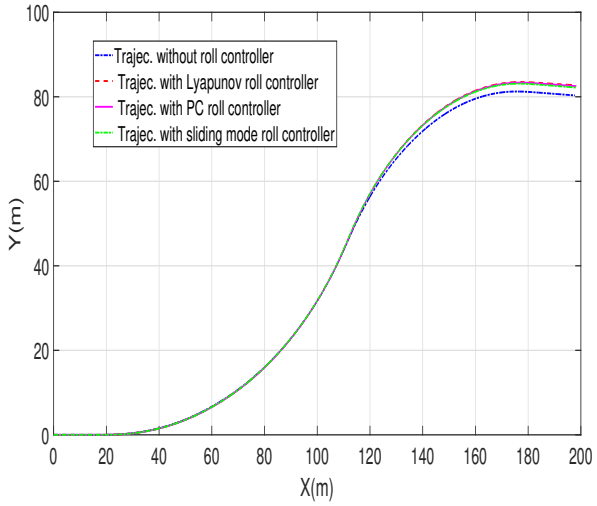

Figure 16: Trajectory comparison; θ_{des} opposite direction

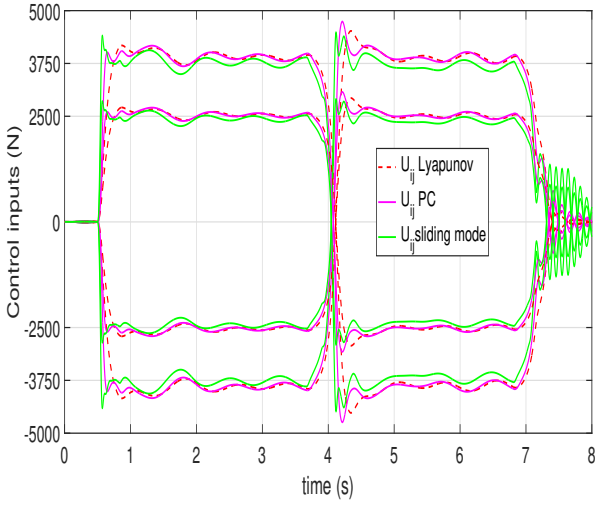

Figure 17: Control inputs comparison: $Asus$ forces; θ_{des} opposite direction

5.2.4 Performance comparison: static vs. dynamic roll reference

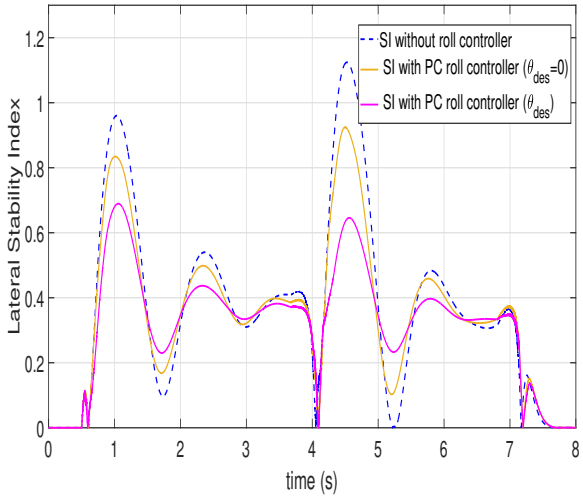

Figure 18: SI comparison; $\theta_{des} = 0$ vs θ_{des} opposite direction

Turning the roll angle in the opposite direction requires more energy compared to simply minimizing it to zero because it necessitates the use of $ASus$ actuators, which consume more energy compared to semi-$ASus$ or Active Roll Bars (ARB) actuators. Moreover, integrating $ASus$ into production vehicles can incur relatively high costs. However, the results of this study demonstrate the effectiveness of $ASus$ in maintaining lateral stability and preventing rollover when the roll angle is controlled in the opposite direction. Figure 18 provides a comparison of the lateral stability index (SI) for the vehicle when controlling the roll angle towards zero and when controlling it towards the desired angle (θ_{des}) using a polynomial control technique. The figure illustrates that controlling the roll angle in the opposite direction yields a greater improvement in lateral stability compared to simply reducing the roll angle to zero. Therefore, this technique has the potential to reduce the energy demand of other actuators utilized for lateral stability, such as AFS and Active Differential Braking (ADB).

5.3 Robustness against parameters variation

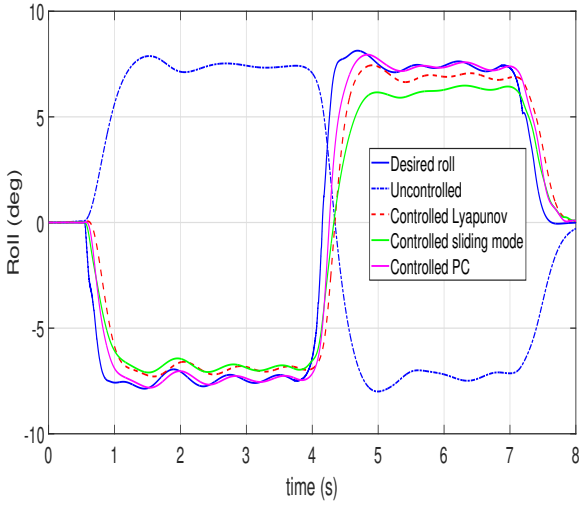

Figure 19: Roll comparison; θ_{des} opposite direction with $M + 30\%$

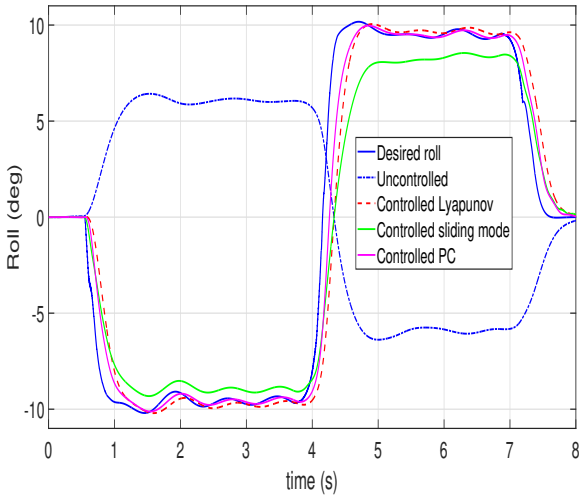

Figure 20: Roll comparison; θ_{des} opposite direction with $h - 10\%$

To evaluate the robustness of the three controllers (Lyapunov, sliding mode, and polynomial) under uncertainty, two types of uncertainties are considered: 1) an increase of 30% in the total vehicle mass M, and 2) a decrease of 10% in the sprung mass roll arm h_θ from their nominal values. The controllers' gains are kept constant throughout the analysis. The roll angle responses to these parametric uncertainties are depicted in Figures 19 and 20. The polynomial controller exhibits varying roll angles during the transient phase but eventually reaches the desired angle. The error rate remains minimal, not exceeding 1%. In contrast, the Lyapunov

controller shows sensitivity to the uncertainties, with a higher error rate of up to 8% when the total vehicle mass M is increased by 30%. This can be attributed to the requirement of accurate knowledge of the components of $M_{\theta_{eq}}$ for generating the control law. The model-free sliding-mode ($STSM$) controller tracks the desired roll trajectory with an error rate of 5% in both cases but exhibits some chattering. Overall, the polynomial controller demonstrates greater robustness against the additional uncertainties, as it is minimally affected by their presence.

6 Conclusion and Perspectives

This study emphasizes the advantages of roll motion control in enhancing vehicle lateral stability and preventing rollover incidents. A polynomial controller was developed to generate the roll moment and effectively regulate the roll angle. A comparison between Lyapunov-based, polynomial, and STSM (Sliding-Mode) controllers demonstrated that the polynomial controller yielded superior and more reliable outcomes while requiring fewer measurements. Furthermore, it was observed that controlling the roll in the opposite direction using active suspensions offered greater benefits in terms of lateral stability and rollover prevention compared to simply minimizing the roll angle to zero.

While active suspensions offer substantial advantages in managing roll motion and enhancing overall vehicle dynamics as seen in the previous subsections, exclusive reliance on them presents certain limitations and challenges. These include the inherent complexities and costs associated with incorporating additional sensors compared to passive suspension systems. The continuous requirement for electrical power to operate active suspension systems contributes to increased power consumption. Furthermore, the addition of weight to the vehicle is a notable drawback of active suspensions. Maintenance and reliability concerns also arise, with the maintenance of active systems potentially being more intricate than that of passive systems. Notwithstanding these challenges, active suspensions continue to stand as a powerful technology for advancing vehicle dynamics, ride quality, and handling. Ongoing technological advancements hold the promise of introducing innovations that may progressively alleviate some of these challenges over time.

In the context of GCC, the roll control system can be activated based on two primary conditions: when the lateral Stability Index (SI) exceeds 0.7 (to enhance lateral stability) and when LTR exceeds 0.8 (to prevent rollover). However, the roll motion control can also be activated at any time without compromising lateral stability or rollover prevention. The activation conditions bring the advantage of minimizing energy consumption by the active suspensions. This necessitates a higher-level decision or supervision layer to coordinate the suspensions with other stabilizing systems such as AFS and DYC within the GCC framework. Integrating the developed roll control into an integrated GCC architecture represents a potential future direction for this research.

Acknowledgements This research work is funded by Agence Nationale de la Recherche (ANR), France, in the context of Project V3EA (Véhicule Electrique, Econome en Energie et Autonome).

References

[1] Bel Haj Frej G, Moreau X, Hamrouni E, Benine-Neta A and Hernette V, Multi-Modes Control for Semi-Active Suspension Systems, *IFAC-PapersOnLine*, 2020, **vol. 53, no. 2**, 14407–14412.

[2] Jin X, Wang J, Sun S, Li S, Yang J and Yan Z, Design of constrained robust controller for active suspension of in-wheel-drive electric vehicles. *Mathematics*, 2021, **9(3)**, 249.

[3] Savaresi S M, Poussot-Vassal C, Spelta C, Sename O and Dugard L Semi-active suspension control design for vehicles. *Elsevier*, 2010.

[4] Meetei L V and Das D K, Enhanced nonlinear disturbance observer based sliding mode control design for a fully active suspension system, *International Journal of Dynamics and Control*, 2021, **9(3)**, 971–984.

[5] Waghmare D B, Asutkar V G and Patre B M, Extended disturbance observer based robust sliding mode control for active suspension system. *International Journal of Dynamics and Control*, 2021 **9(4)**, 1681–1694.

[6] Doumiati M, Sename O, Dugard L, Martinez-Molina J J, Gaspar P and Szabo, Z, Integrated vehicle dynamics control via coordination of active front steering and rear braking. *European Journal of Control*,2013, **19(2)**, 121—143.

[7] Solmaz S, Corless M and Shorten R, A methodology for the design of robust rollover prevention controllers for automotive vehicles with active steering. *International Journal of Control*, 2007 **80(11)**, 1763—1779.

[8] Bouvin J L, Hamrouni E, Moreau X, Benine-Neto A, Hernette V, Serrier P and Oustaloup A, Hierarchical approach for Global Chassis Control. *2018 European Control Conference (ECC)*, 2018, 2555–2560.

[9] Akhmetov Y, Remond D, Maiffredy L, Di Loreto M, Marquis-Favre W and Harth V, Global Chassis Control for active safety of heavy vehicles. *World Automotive Congress FISITA*, 2010.

[10] Liu W, He H, Sun F and Lv J, Integrated chassis control for a three-axle electric bus with distributed driving motors and active rear steering system. *Vehicle System Dynamics*, 2017, **55(5)**, 601–625.

[11] Dahmani H, Chadli M, Rabhi A and El hajjaji A, Detection of impending vehicle rollover with road bank angle consideration using a robust fuzzy observer, *International Journal of Automation and Computing*, 2015, **12**, 93-–101.

[12] Li Y, Sun W, Huang J, Zheng L and Wang Y, Effect of vertical and lateral coupling between tyre and road on vehicle rollover, *Vehicle System Dynamics*,2013, **51(8)**, 1216—1241.

[13] Luo J, Li P, Li P and Cai Q, Observer-based multi-objective integrated control for vehicle lateral stability and active suspension design, *Journal of Sound and Vibration*,2021, **508**, 116222.

[14] Ataei M, Khajepour A and Jeon S, Model predictive control for integrated lateral stability, traction/braking control, and rollover prevention of electric vehicles, *Vehicle system dynamics*, 2020, **58(1)**, 49-–73.

[15] Vivas-Lopez C A, Tudon-Martinez J C, Hernandez-Alcantara, D and Morales-Menendez R, Global chassis control system using suspension, steering, and braking subsystems, *Mathematical Problems in Engineering*, 2015.

[16] Zhao S.E, Li Y and Qu X, Vehicle chassis integrated control based on multimodel and multilevel

hierarchical control, *Mathematical Problems in Engineering*, 2014.

[17] Cronje P H and Els P S, Improving off-road vehicle handling using an active anti-roll bar, *Journal of Terramechanics, Elsevier*, 2010, **47(3)**, 179-–189.

[18] Vu V T, Tran V D, Pham Q T, Truong M H, Sename O and Gáspár P, Designing LQR controllers for an active anti-roll bar system with a flexible frame model of a single unit heavy vehicle, *Periodica Polytechnica Transportation Engineering*, 2021, **49(3)**, 199–209.

[19] Yao J, Lv G, Qv M, Li Z, Ren S and Taheri S, Lateral stability control based on the roll moment distribution using a semiactive suspension, *Proceedings of the Institution of Mechanical Engineers, Part D: Journal of Automobile Engineering*, 2017, **231(12)**, 1627—1639.

[20] Fergani S, Menhour L, Sename O, Dugard L and D'Andréa-Novel B, Integrated vehicle control through the coordination of longitudinal/lateral and vertical dynamics controllers: Flatness and lpv/-based design, *International Journal of Robust and Nonlinear Control*, 2017, **27(18)**, 4992—5007.

[21] Chokor A, Talj R, Doumiati M and Charara A, Effect of Roll Motion Control on Vehicle Lateral Stability and Rollover Avoidance, *American Control Conference, Denver, United States*, 2020, 4868–4875.

[22] Chokor A, Talj R, Doumiati M, Hamdan A and Charara A, A comparison between a centralized multilayer lpv/hinfinity and a decentralized multilayer sliding mode control architectures for vehicle's global chassis control, *International Journal of Control*, 2020, DOI: 10.1080/00207179.2020.1791360.

[23] Kim C and Huh K, Active Roll Control System Design With Considering Actuator Constraints for Passenger Car, Active Roll Control System Design With Considering Actuator Constraints for Passenger Car, *Journal of Dynamics Systems, Measurement, and Control*, 2019, **vol 141(12)**, https://doi.org/10.1007/s13369-022-07267-6.

[24] Prakash R and Dheer D K, Evolutionary Algorithms Based Model Predictive Control for Vehicle Lateral and Roll Motion Control, *Arab. Arab J Sci Eng*, Springer, 2023 2023, https://doi.org/10.1007/s13369-022-07267-6

[25] Hu X, Wang P, Cai S, Zhang L, Hu Y and Chen H, Vehicle Stability Analysis by Zero Dynamics to Improve Control Performance, *IEEE Transactions on Control Systems Technology*, 2023, doi: 10.1109/TCST.2023.3257682.

[26] Tanaka K, Yoshida H, Ohtake H and Wang H O, A sum of squares approach to stability analysis of polynomial fuzzy systems, *In 2007 American Control Conference*, 2007, 4071–4076.

[27] Prajna S, Papachristodoulou A and Parrilo P A, SOSTOOLS: sum of squares optimization toolbox for MATLAB–user's guide, *Control and Dynamical Systems, California Institute of Technology, Pasadena, CA*,2004, **91125**.

[28] Liu W, He H, Sun F and Lv J, Nonlinear state-feedback design for vehicle lateral control using sum-of-squares programming, *Vehicle System Dynamics*, 2022, **60(3)**, 743–769.

[29] Pacejka, Tire and vehicle dynamics, 3rd edition, *Elsevier*, 2012.

[30] Rajamani R, Vehicle Dynamics and Control, *Springer*, 2012.

[31] Doumiati M, Charara A, Victorino A and Lechner D, Vehicle dynamics estimation using Kalman filtering: experimental validation, *John Wiley & Sons*, 2012.

[32] Chokor A, Talj R, Charara A, Shraim H and Francis C, Active suspension control to improve passengers comfort and vehicle's stability, *19th IEEE International Conference on Intelligent Transportation Systems (ITSC)*, 2016, 296—301.

[33] Chokor A, Talj R, Charara A, Doumiati M and Rabhi A, Rollover prevention using active suspension system, *20th IEEE International Conference on Intelligent Transportation Systems (ITSC)*, 2017, 1706-–1711.

[34] Vu V T, Sename O, Dugard L and Gaspar P, Enhancing roll stability of heavy vehicle by lqr active anti-roll bar control using electronic servo-valve hydraulic actuators, *Vehicle System Dynamics*, 2017, **55(9)**, 1405-–1429.

[35] Gillespie T D, Fundamentals of Vehicle Dynamics, Revised Edition, *SAE International*, 2021, ISBN of 978-1-4686-0176-3.

[36] National Highway Traffic Safety Administration, *Department of Transportation National Highway Traffic Safety Administration*, https://www-fars.nhtsa.dot.gov/, 2020.

[37] Ungoren A Y and Peng H, Evaluation of vehicle dynamic control for rollover prevention, *International Journal of Automotive Technology*, 2004, **5(2)**, 115-–122.

[38] Iben Ammar I, Gassara H, El Hajjaji A and Chaabane M, DC-DC Buck Converter Polynomial Tracking Control Design With Saturation Constraint, *2021 60th IEEE Conference on Decision and Control (CDC)*, 2021, IEEE, 2800–2805.

[39] Lam H K, Output-feedback tracking control for polynomial fuzzy model-based control systems, *In Polynomial Fuzzy Model-Based Control Systems*, 2016, 175–196.

[40] Rakhshan M, Vafamand N, Khooban M H and Blaabjerg F, Maximum power point tracking control of photovoltaic systems: A polynomial fuzzy model-based approach, *IEEE Journal of Emerging and Selected Topics in Power Electronics*, 2017, 292–299.

[41] Vafamand N, Rakhshan M, Dynamic model-based fuzzy controller for Maximum Power Point Tracking of Photovoltaic Systems: A Linear Matrix Inequality Approach, *Journal of Dynamic Systems, Measurement and control*, 2017; 139(5): 051010. https://doi.org/10.1115/1.4035240.

[42] Ksander N. de Winkel, T. Irmak, R. Happee, B. Shyrokau, *Standards for passenger comfort in automated vehicles: Acceleration and jerk*, Applied Ergonomics, Elsevier, 2023.

[43] Slotine J.J , Li Weiping, *Applied nonlinear control*, ISBN : 0-13-040890-5, Pearson 1991.

[44] SCANeR, SCANeR studio simulator, Online, *Available: https://www.avsimulation.com/scaner/*.

[45] B. Borchers. CSDP, Library for semidefinite programming, *Optimization Methods and Software*, 11(1–4):613–623, 1999.

[46] J. F. Sturm. Using SeDuMi 1.02, A MATLAB toolbox for optimization over symmetric cones, *Optimization Methods and Software, 11–12:625–653*, 1999.

7 Appendix

7.1 Proof of stability

A stabilizing feedback gain $\mathbb{K}(\theta)$ can be obtained from $P(\overline{\widetilde{x}})$ and $Z(\theta)$ as $\mathbb{K}(\theta) = Z(\theta)P^{-1}(\overline{\widetilde{x}})$ [38].

Proof The constraints (37) guarantee the positive-definiteness of $P(\overline{\widetilde{x}})$.

At first part of the proof, we will prove that condition (38) assurances the set inclusion as follow

$$\gamma(P^{-1}(\overline{\widetilde{x}}), 1) \subset L(Y(\widetilde{x}), M_{\theta,\max}) \tag{52}$$

This result on the one hand, $\forall \widetilde{x} \in \gamma(P^{-1}(\overline{\widetilde{x}}), 1)$, the following inequality

$$2M_{\theta,\max_r} \geq M_{\theta,\max_r}(1 + \widetilde{x}^T P^{-1}(\overline{\widetilde{x}})\widetilde{x}) \geq 2|Y_r(\widetilde{x})\widetilde{x}|, \forall r = 1, ..., n_{M_\theta} \tag{53}$$

where $Y_r(\widetilde{x})$ denotes the rth row of $Y(\widetilde{x})$ and $M_{\theta,\max_r}$ is the rth row of $M_{\theta,\max}$.
implies that

$$|Y_r(\widetilde{x})\widetilde{x}| \geq M_{\theta,\max_r}, \forall r = 1, ..., n_{M_\theta} \tag{54}$$

On the other hand, condition (38) implies that

$$\begin{bmatrix} M^2_{\theta,\max_r} & T_r(\widetilde{x}) \\ * & P(\overline{\widetilde{x}}) \end{bmatrix} > 0 \tag{55}$$

Define $Y_r(\widetilde{x}) = T_r(\widetilde{x})P^{-1}(\overline{\widetilde{x}})$. Pre and post-multiplying both side of (55) by $\begin{bmatrix} \frac{1}{\sqrt{M_{\theta,\max_r}}} & 0 \\ 0 & \sqrt{M_{\theta,\max_r}}P^{-1}(\overline{\widetilde{x}}) \end{bmatrix}$ and its transpose, we obtain

$$\begin{bmatrix} M_{\theta,\max_r} & Y_r(\widetilde{x}) \\ * & M_{\theta,\max_r}P^{-1}(\overline{\widetilde{x}}) \end{bmatrix} > 0 \tag{56}$$

which implies that

$$\begin{bmatrix} 1 & \pm\widetilde{x}^T \end{bmatrix} \begin{bmatrix} M_{\theta,\max_r} & Y_r(\widetilde{x}) \\ * & M_{\theta,\max_r}P^{-1}(\overline{\widetilde{x}}) \end{bmatrix} \begin{bmatrix} 1 \\ \pm\widetilde{x} \end{bmatrix} \geq 0 \tag{57}$$

This can be rewritten as follows:

$$M_{\theta,\max_r}(1 + \widetilde{x}^T P^{-1}(\overline{\widetilde{x}})\widetilde{x}) \geq 2|Y_r(\widetilde{x})\widetilde{x}| \tag{58}$$

This completes the first part of the proof.
We can calculate $\dot{V}(\widetilde{x})$ as follows :

$$\begin{aligned} \dot{V}(\widetilde{x}) =& \widetilde{x}^T(\mathbb{H}^T(\theta)P^{-1}(\overline{\widetilde{x}}) + P^{-1}(\overline{\widetilde{x}})\mathbb{H}(\theta) + \sum_{q=1}^{Q} \frac{\partial P^{-1}(\overline{\widetilde{x}})}{\partial \widetilde{x}_q}\mathbb{A}^q(\theta)\widetilde{x})\widetilde{x} \\ &+ \widetilde{x}^T P^{-1}(\overline{\widetilde{x}})(\mathbb{G}_1 F_{fr} + \mathbb{G}_2 F_{fl} + \mathbb{G}_3 F_{rr} + \mathbb{G}_4 F_{rl} + \mathbb{G}_5(\theta, z_s)a_y + \mathbb{G}_6 z_s + \mathbb{G}_7\theta_{des}) \\ &+ (\mathbb{G}_1 F_{fr} + \mathbb{G}_2 F_{fl} + \mathbb{G}_3 F_{rr} + \mathbb{G}_4 F_{rl} + \mathbb{G}_5(\theta, z_s)a_y + \mathbb{G}_6 z_s + \mathbb{G}_7\theta_{des})^T P^{-1}(\overline{\widetilde{x}})\widetilde{x} \end{aligned} \tag{59}$$

where $\mathbb{A}^j(\theta)$ signify the jth row of $\mathbb{A}(\theta)$.

$$\begin{aligned} \dot{V}(\widetilde{x}_1) \leq& \widetilde{x}^T(\mathbb{H}^T(\theta)P^{-1}(\overline{\widetilde{x}}) + P^{-1}(\overline{\widetilde{x}})\mathbb{H}(\theta) + \sum_{q=1}^{Q} \frac{\partial P^{-1}(\overline{\widetilde{x}})}{\partial \widetilde{x}_q}\mathbb{A}_1^q(\theta)\widetilde{x})\widetilde{x} \\ &+ \widetilde{x}^T P^{-1}(\overline{\widetilde{x}})(\mathbb{G}_1\mathbb{G}_1^T + \mathbb{G}_2\mathbb{G}_2^T + \mathbb{G}_3\mathbb{G}_3^T + \mathbb{G}_4\mathbb{G}_4^T + \mathbb{G}_5(\theta, z_s)\mathbb{G}_5(\theta, z_s)^T + \mathbb{G}_6\mathbb{G}_6^T \\ &+ \mathbb{G}_7\mathbb{G}_7^T)P^{-1}(\overline{\widetilde{x}})\widetilde{x} + F_{fr}^T F_{fr} + F_{fl}^T F_{fl} + F_{rr}^T F_{rr} + F_{rl}^T F_{rl} + a_y^T a_y + z_s^T z_s + \theta_{des}^T\theta_{des} \end{aligned} \tag{60}$$

If the controller gain yield :

$$\begin{aligned}&\mathbb{H}^T(\theta)P^{-1}(\overline{\widetilde{x}})+P^{-1}(\overline{\widetilde{x}})\mathbb{H}(\theta)+\sum_{q=1}^{Q}\frac{\partial P^{-1}(\overline{\widetilde{x}})}{\partial\widetilde{x}_q}\mathbb{A}^q(\theta)\widetilde{x}+P^{-1}(\overline{\widetilde{x}})(\mathbb{G}_1\mathbb{G}_1^T+\mathbb{G}_2\mathbb{G}_2^T+\mathbb{G}_3\mathbb{G}_3^T\\&+\mathbb{G}_4\mathbb{G}_4^T+\mathbb{G}_5(\theta,z_s)\mathbb{G}_5(\theta,z_s)^T+\mathbb{G}_6\mathbb{G}_6^T+\mathbb{G}_7\mathbb{G}_7^T)P^{-1}(\overline{\widetilde{x}})+\overline{S}\leq 0\end{aligned}\tag{61}$$

For $\overline{S}=\overline{S}^T>0$, then

$$\dot{V}(\widetilde{x})\leq-\widetilde{x}\overline{S}\widetilde{x}+F_{fr}^TF_{fr}+F_{fl}^TF_{fl}+F_{rr}^TF_{rr}+F_{rl}^TF_{rl}+a_y^Ta_y+z_s^Tz_s+\theta_{des}^T\theta_{des}\tag{62}$$

This implies that $\dot{V}(\widetilde{x})\leq 0$ for $\lambda_{\min}(\overline{S})\|\widetilde{x}\|^2\geq\|F_{fr}\|^2+\|F_{fl}\|^2+\|F_{rr}\|^2+\|F_{rl}\|^2+\|a_y\|^2+\|z_s\|^2+\|\theta_{des}\|^2$ (where $\lambda_{\min}(.)$ denotes a minimum eigenvalue operator).
Next we show that the stability condition (61) is equivalent to the SOS condition (39).
The constraint (39) implies

$$\begin{bmatrix}\Omega^1(\widetilde{x}) & P(\overline{\widetilde{x}})S\\ SP(\overline{\widetilde{x}}) & -P(\overline{\widetilde{x}})\end{bmatrix}>0\tag{63}$$

By letting $\overline{S}=SP^{-1}(\overline{\widetilde{x}})S$ and applying Schur complement to (63), we obtain :

$$\Omega^1(\widetilde{x})+P(\overline{\widetilde{x}})SP^{-1}(\overline{\widetilde{x}})SP(\overline{\widetilde{x}})\leq 0\tag{64}$$

Define $\mathbb{K}(\theta)=Z(\theta)P^{-1}(\overline{\widetilde{x}})$ and $\mathbb{Y}(\theta)=T(\theta)P^{-1}(\overline{\widetilde{x}})$. Pre- and post-multiplying the last expression by $P^{-1}(\overline{\widetilde{x}})$, we obtain:

$$\begin{aligned}&\mathbb{H}^T(\theta)P^{-1}(\overline{\widetilde{x}})+P^{-1}(\overline{\widetilde{x}})\mathbb{H}(\theta)+\sum_{q=1}^{Q}\frac{\partial P^{-1}(\overline{\widetilde{x}})}{\partial\widetilde{x}_q}\mathbb{A}^q(\theta)\widetilde{x}\\&+P^{-1}(\overline{\widetilde{x}})(\mathbb{G}_1\mathbb{G}_1^T+\mathbb{G}_2\mathbb{G}_2^T+\mathbb{G}_3\mathbb{G}_3^T+\mathbb{G}_4\mathbb{G}_4^T+\mathbb{G}_5(\theta,z_s)\mathbb{G}_5(\theta,z_s)^T+\mathbb{G}_6\mathbb{G}_6^T\\&+\mathbb{G}_7\mathbb{G}_7^T)P^{-1}(\overline{\widetilde{x}})+\overline{S}\leq 0\end{aligned}\tag{65}$$

Therefore, (39) implies that $\dot{V}(\widetilde{x})\leq 0$.

7.2 Vehicle parameters

Table 1 Vehicle parameters

Symbol	Description	**Value**
$m_{s,ij}$	Sprung mass mass at the corner ij	281.6$[kg]$
$m_{us,ij}$	Unsprung mass mass at the corner ij	40$[kg]$
$K_{s,fr}$, $K_{s,fl}$	Suspension stiffness coefficient (front tires)	20000$[N/m]$
$K_{s,rr}$, $K_{s,rl}$	Suspension stiffness coefficient (rear tires)	13000$[N/m]$
$C_{s,fr}$, $C_{s,fl}$	Suspension damping coefficient (front tires)	9830$[N.s/m]$
$C_{s,rr}$, $C_{s,rl}$	Suspension damping coefficient (rear tires)	3000$[N.s/m]$
K_t	Tire stiffness coefficient	467000$[N/m]$
C_t	Tire damping coefficient	500$[N.s/m]$
t_f	Half front track	0.773$[m]$
t_r	Half rear track	0.773$[m]$
l_f	Wheelbase to the front	1.0385$[m]$
l_r	Wheelbase to the rear	1.6015$[m]$
h	Height of the vehicle CG	0.58$[m]$
h_r	Height of the unsprung mass CG	0.31$[m]$
h_θ	Sprung mass roll arm	0.27$[m]$
h_ϕ	Sprung mass pitch arm	0.27$[m]$
M	Total vehicle mass	1286.4$[kg]$
M_s	Sprung mass	1126.4$[kg]$
I_x	Roll moment of inertia of sprung mass	534$[kg.m^2]$
I_y	Pitch moment of inertia of sprung mass	1860$[kg.m^2]$
I_z	Vehicle yaw moment of inertia	1970$[kg.m^2]$
I_{xz}	Vehicle yaw-roll product of inertia	743$[kg.m^2]$
g	Gravity constant	9.81$[m/s^2]$
μ	Road adherence coefficient	dry surface= 1
C_f, C_r	Front, rear tire cornering stiffness (bicycle model)	76776$[N/rad]$
K_θ	Roll suspension angular stiffness	30000$[N.m/s]$
C_θ	Roll suspension angular damper	10000$[N.m/s]$